

Draft of April 24, 2022

Published as:

Farfan GA, Zhou C, Valley JW, Orland IJ (2021) Coupling Mineralogy and Oxygen Isotopes to Seasonal Environmental Shifts Recorded in Modern Freshwater Pearl Nacre from Kentucky Lake. *Geochem Geophys Geosyst*, 22, 12, 17p, doi.org/10.1029/2021GC009995.

The role of organics and crystal structure on pearl nacre geochemistry, cathodoluminescence, and Raman signals

Gabriela A. Farfan¹, Emma Bullock², Chunhui Zhou³, John W. Valley⁴

¹Department of Mineral Sciences, National Museum of Natural History, Smithsonian Institution, Washington, DC, 20560

²Earth and Planets Laboratory, Carnegie Institution for Science, Washington, DC, 20015

³Gemological Institute of America, New York, NY 10036

⁴Department of Geoscience, University of Wisconsin, Madison, WI 53706

Introduction

Empirically-based biomineral paleoproxies are very important chemical tools used to trace past climate. Like tree rings, the layered nature of aragonite nacre growth preserves a record of the conditions during growth. Nacre lends itself to being used in paleoproxies for temperature and pressure based on oxygen isotopes (e.g., Rousseau & Rollion-Bard, 2012; Linzmeier et al., 2018; Farfan et al. 2021), tablet thickness (Rousseau & Rollion-Bard, 2012; Olson et al., 2012; Gilbert et al., 2017; Farfan et al. 2021), and even tablet orientation (Olson & Gilbert, 2012; Farfan et al. 2021). Yet, the relationship between isotopic compositions and trace element chemistry and how they relate to kinetics of crystallization, crystal structure and trapped organic molecules in nacre is still an active topic of research. A combined mineralogical-geochemical approach using ultrahigh-resolution mapping via cathodoluminescence, electron microprobe, SIMS, and Raman spectroscopy offers a new perspective to help interpret and support these proxies based on crystal chemistry and structure. Modern farmed (“cultured”) freshwater pearls provide pristine time capsules of nacre of known ages that can aid in our understanding these relationships. Beyond testing their reliability as paleoproxies, understanding how pearl nacre is impacted by shifts in climate and local environments is also important for predicting the health of mollusks and the quality of pearls in the future.

Pearls hold historical and contemporary significance in the world of gems and jewelry, contributing approximately 0.5–1 billion dollars (US) per year to the world’s economy over the past 30 years (Southgate & Lucas 2011; van der Schatte Olivier, 2020). The nacre that makes up pearls and gives them their classic pearlescent luster is a unique biomineral material formed from tablets of aragonite (CaCO_3) stacked together like bricks and interlaid with biological molecules, such as β -chitin and acidic proteins, that serve as the mortar (Addadi and Weiner 1997). Despite containing only up to ~5 wt % organics (Gilbert et al. 2005), being a composite material gives nacre incredible physical properties compared to its abiological aragonite counterparts, such as additional toughness and pearlescent luster (e.g. Addadi et al., 2006; Espinosa et al. 2011;

Barthelat et al. 2016; Gim et al., 2019). This has led materials scientists and engineers to explore nacre for uses in bioinspired materials, for example, their self-healing symmetry properties in nacre has applications for future material technologies (Gim et al. 2021).

In this study, we explore how organics and trace element signals are trapped in natural nacre from freshwater pearls via state-of-the-art ultrahigh-resolution cathodoluminescence (CL) imaging and Raman spectroscopy mapping. These observations help to inform the influence of organics and mineralogy on $\delta^{18}\text{O}$ -based temperature proxies and how all of these variables are be influenced by seasonally-shifting environmental conditions.

Results and Discussion

Heterogeneity of freshwater nacre at μm -scale resolution

While past studies have demonstrated how the chemical and mineralogical heterogeneity of nacre reflects average (Olson et al., 2012; Gilbert et al., 2017) and seasonal (Farfan et al. 2021) shifts in environment at high spatial resolution, this study shows an even higher level of heterogeneity recorded by freshwater pearl nacre on a sub-seasonal scale that is evidenced by geochemical and mineralogical maps using 1–3 μm pixel spatial resolution across a pearl transect. In particular, cathodoluminescence (CL) imaging offers a unique perspective to studying biominerals because it produces different wavelengths of light according to the specific mineral and different activators or structural defects, which are commonly associated with specific modes of formation or alteration, such as aragonite formed by biological processes (Barbin, 2000; England et al. 2006; Toffolo et al. 2019; 2021). Total CL counts at 1×1 μm resolution are mapped across a transect of a pearl cross-section (Figure 1A,B). This approach reveals that the CL signals are highly heterogeneous and follow smooth, fine layer patterns within the pearl, mimicking the layered growth history of the nacre tablets. Overall patterns of CL intensity and colors are mirrored across the pearl nucleus, indicating that these patterns are most likely a result of the nacre growth history and not a random occurrence. The CL signal in this freshwater pearl is dominated by blue and green wavelengths that mix to form an overall teal color, similar to that described in Toffolo et al. 2019 (and green observed in Barbin 2013). An average spectrum for the entire map is presented in Figure 1C in the estimated teal color (#7FB097). Some regions of the pearl are dominated by stronger green wavelengths (outlined as G1 and G2, Fig. 1B), while others favor the blue wavelengths (B1 and B2). Spectra for these specific regions are also presented in Figure 1C with the peak positions for the dominant peaks outlined in their resulting colors (444.4 nm blue and 551.6 nm green). This sub-seasonal heterogeneity is presented alongside all mineralogical and geochemical measurements, and lake environmental data from Kentucky Lake as 2-dimensional transects across the pearl space in Supporting Information, Figure S1.

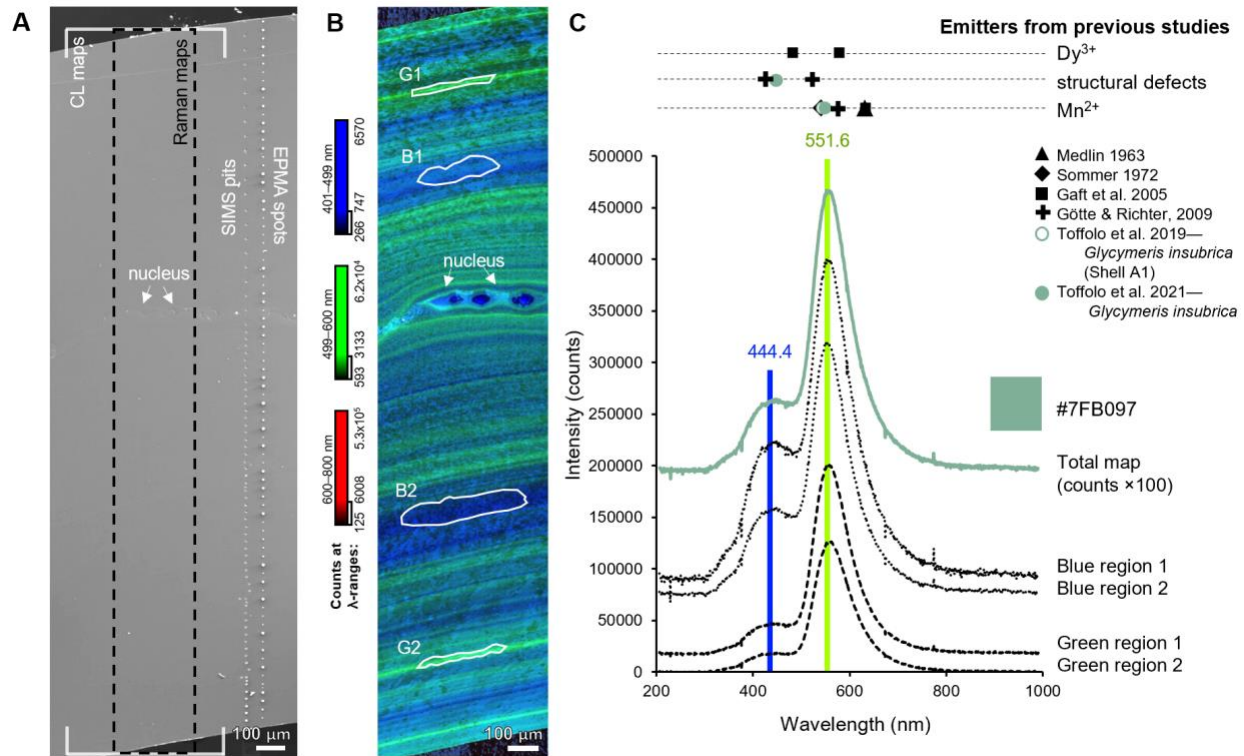


Figure 1. A cross section of a freshwater pearl analyzed by a suite of geochemical and mineralogical techniques. A) A scanning electron micrograph of the pearl cross section showing regions analyzed by cathodoluminescence (CL) maps, Raman spectroscopy maps, secondary ion mass spectrometry (SIMS) transect (Farfan et al. 2021), and electron probe micro-analysis (EPMA) transect. B) A map of total CL counts taken at $1 \times 1 \mu\text{m}$ pixel resolution represented in blue (401–499 nm), green (499–600 nm), and red (600–800 nm) wavelength ranges showing layer features that mirror across the nucleus. Regions outlined in white, “G1” and “G2” represent areas of the map that are particularly strong in green colors, while regions “B1” and “B2” represent strong blue areas. C) Representative CL spectra showing an average spectrum for the total CL map in the estimated teal color (#7FB097). Spectra of blue regions 1 and 2 and green regions 1 and 2 are presented in dotted and dashed black lines, respectively. Peak positions for the two peaks are highlighted in the estimated color for that corresponding wavelength (blue for 444.4 nm and green for 551.6 nm). Positions of CL peaks from previous aragonite studies with their associated emitters are presented above the spectra in this study.

The role of organics in nacre geochemistry and mineralogy

A ultrahigh-resolution CL map representing the region of the spectrum that corresponds to the dominant CL peak at 551.6 nm (Fig. 2A) displays a heterogeneous layer pattern that is very similar to the total CL map (Fig. 1B, $R^2=0.98$ between CL total and CL 551 nm). It also resembles the same patterns observed in a WDS map of Mn concentrations and is strongly correlated with these values (Fig. 2B, D; $R^2=0.44$, $R=0.66$). This correlation between the 551 nm CL signal and Mn distributions is in agreement with previous studies that suggest that Mn^{2+} is the emitter responsible for this dominant CL signal in biogenic aragonite and calcite (Fig. 1C; Sommer et al. 1972; Narasimhulu and Rao, 2000; Götte and Richter, 2009; Toffolo et al. 2019;

2021). This Mn²⁺-based CL signal is so distinctive that it has even been used to identify the provenance of freshwater pearls from the Mississippi River region, USA versus those from China (Banerjee, A., & Habermann, 2002). In various shells, the Mn²⁺ is shown to be most likely a combination of organically-bound Mn²⁺ and mineral-bound Mn²⁺ (substitutions for Ca²⁺ in aragonite and as calcite-structure micro-domains, as shown by XANES), although the precise bonding environment is still an active topic of research (e.g. Carré et al. 2006; Soldati et al. 2010; 2016; Toffolo et al., 2021). In estuarine *Corbula amurensis* shells, oxidative treatments revealed that a large fraction (78%) of total Mn is associated with organics and that this organically-bound fraction could complicate traditional proxy relationships (Takesue et al. 2008). Since manganese is an important co-factor in many enzymes essential for life, organically-bound Mn²⁺ is an unsurprising occurrence in nacre and shells (Hänsch and Mendel, 2009). Mn²⁺ concentrations are also observed to preserve seasonal cycles within shells, with elevated concentrations occurring in higher organic:mineral summer shell layers that could potentially make Mn concentrations in shells a useful proxy for primary productivity and Mn concentrations in lakes (Jeffree et al. 1995; Siegele et al 2001; Soldati et al. 2009).

In addition to being closely correlated with Mn-distributions, we observe that the 551 nm CL signal is also correlated to the pearl nacre Raman background luminescence signal, herein referred to as background fluorescence and presented here as the ratio of background fluorescence:v₁ mode peak height (Fig. 2B,E; R²=0.35). This background fluorescence signal in biocarbonates is assumed to represent organic compounds which commonly emit strong fluorescence (Cuif et al. 2014; DeCarlo et al. 2018). Thus, we assume that the background fluorescence from other potential abiogenic emitters is negligible compared to the organic-driven signal. If this assumption holds, due to the strong positive correlations between the 551 CL signal, Mn distributions, and Raman background fluorescence (Fig. 2D,E), we propose that a significant portion of the Mn in this pearl nacre is predominantly organically-bound, in addition to the Mn²⁺ substituted within the aragonite structure. To further strengthen this concept, if we assume that the thickness of the organic interlayers between nacre tablets remains consistent, like mortar between bricks, we would expect regions of nacre with thicker tablets to contain lower organic contents compared to regions with more layers of thinner tablets. This is precisely what we observe, with nacre tablet thickness moderately negatively correlating with the organics-associated 551 nm CL signal (Fig. 2F; R²=0.19, R= -0.44) and Raman fluorescence (R²=0.15, R= -0.38).

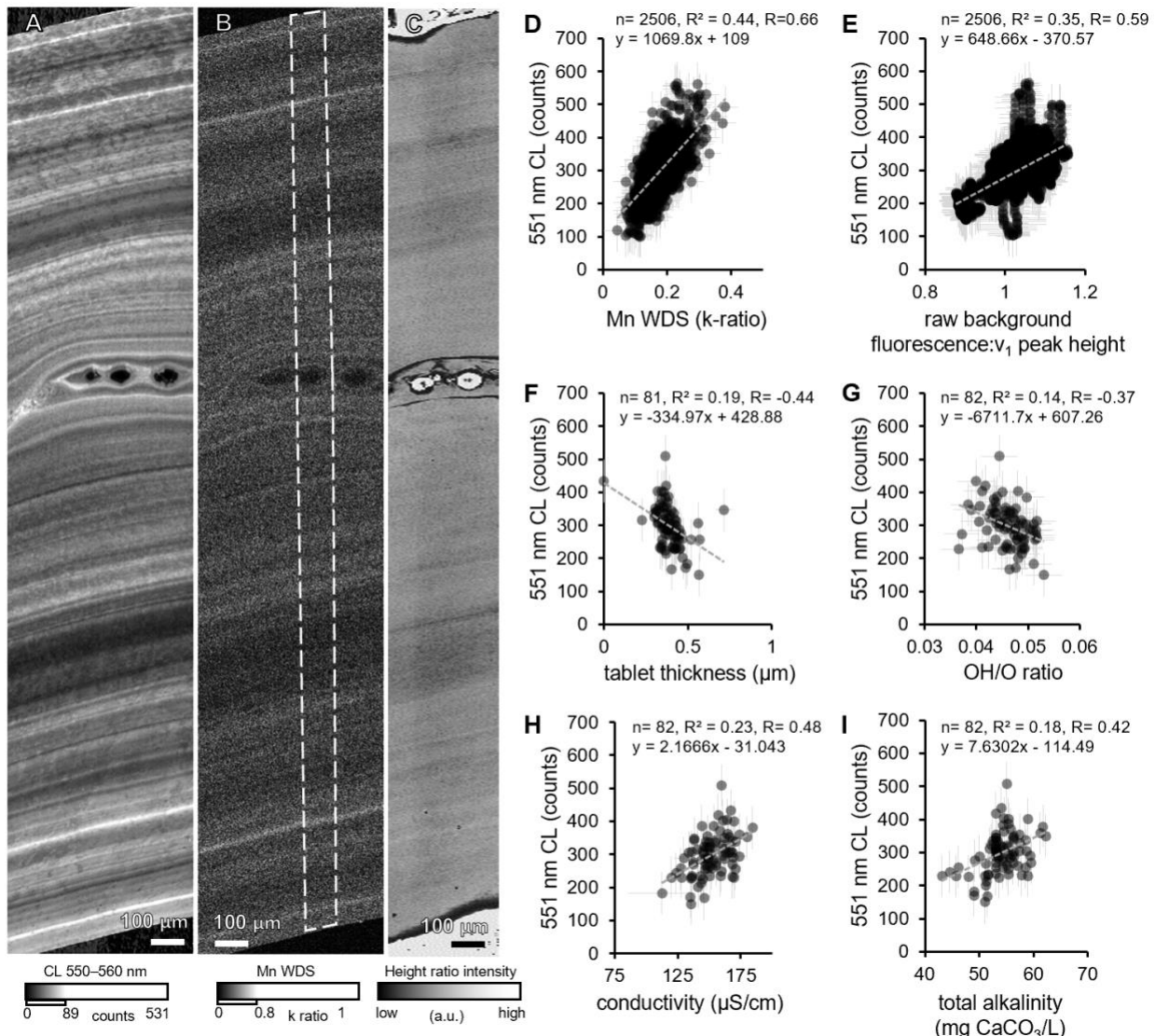


Figure 2. Ultra-high resolution maps of A) CL counts for the 550–560 nm wavelengths that represent the dominant 551 nm CL peak collected at 1×1 µm pixel resolution. B) Mn distributions by WDS mapping expressed as k-ratios collected at 1×1 µm pixel resolution. The dashed white line represents the region that was integrated to give two-dimensional transects to compare with other variables. Maps for other elements (EDS and WDS) can be found in the Supporting Information, Figure S2. C) Ratio of background fluorescence:v₁ mode peak height at 3×6 µm pixel resolution. Note that the edges of the pearl have extra background fluorescence signal leaking from the surrounding epoxy that interrupts the true signal in these regions. Other Raman fluorescence maps can be found in the Supporting Information, Figure S6. Relationships between the 551 nm CL signal as a function D) Mn WDS values, E) background fluorescence:v₁ mode peak height, F) nacre tablet thickness, G) nacre OH/O ratios, H) lake conductivity, and I) lake total alkalinity. Values for tablet thickness, OH/O ratios and lake conductivity and total alkalinity are from Farfan et al. (2021). All values can be accessed in Supporting Information

Table S1 and statistical significance (p-values), Pearson correlation coefficients (R), and linear regressions (R^2) between all variables in this study are in Supporting Information Table S3.

Implications for the $\delta^{18}\text{O}_{\text{Arg}}$ temperature proxy

In contrast to the positive correlation between the 551 nm CL signal and Raman fluorescence from organics, we observe that SIMS-based nacre OH/O ratios, proposed to be from organic or hydrous components (Linzmeier et al. 2016; Orland et al. 2015; Wycech et al. 2018), are actually negatively correlated with the 551 nm CL signal (Fig. 2G; $R^2=0.14$, $R= -0.37$) and positively correlated with increasing tablet thickness (Farfan et al. 2021). Considering that it is still unknown whether the OH in nacre is from organics molecules vs. OH-groups or water trapped around the aragonite tablets, our results here suggest that OH is likely not associated with organics. Nacre OH/O values are closely linked with nacre aragonite $\delta^{18}\text{O}$ values ($\delta^{18}\text{O}_{\text{Arg}}$; measured at 10- μm scale by SIMS, Farfan et al. 2021) and we observe no clear correlations between $\delta^{18}\text{O}_{\text{Arg}}$ and any CL signals, Raman fluorescence, or Mn concentrations in this study that would be traditionally associated with organic contents. This may indicate that $\delta^{18}\text{O}_{\text{Arg}}$ values are not tied to organic contents in freshwater pearl nacre and do accurately record lake $\delta^{18}\text{O}$ signals that reflect temperature and dissolved oxygen conditions in Kentucky Lake. However, there does appear to be an offset between the seasonal nacre-based $\delta^{18}\text{O}_{\text{Arg}}$ peaks that lag behind peaks for the 551 nm CL signal and Mn concentrations in the nacre (Supporting Information, Figure S1; 551 nm CL peaks highlighted in blue bars). Thus, the organic contents in nacre may be shifting before the seasons reach their peak temperatures, as recorded by the oxygen isotopes.

Alternatively, previous studies have discussed that oxygen isotope signals in mollusk shells are often delayed days to weeks from the true temperature peaks, thus, the organics (and the 551 nm CL signal) may better signal true time points within the nacre (e.g. Vihtakari et al. 2016). Unlike previous studies that observed higher Mn and organics in summer layers (Jeffree et al. 1995; Siegele et al 2001; Soldati et al. 2010), if we were to offset the oxygen isotopes and temperature transects to match with Mn and CL signals, we find that the higher organics and Mn are aligned with cold, winter peaks, as opposed to summer peaks. This needs to be further explored and accounted for with future controlled incubation studies. Without offsetting the environmental data, the organics-associated 551 nm CL signal is most closely correlated with conductivity (a measure of ionic strength; Fig. 2H; $R^2=0.23$, $R= 0.48$) and total alkalinity (Fig. 2I; $R^2=0.18$, $R= 0.42$) in Kentucky Lake (Supporting Information, Figure S1).

Morphological and crystal structure shifts in pearl nacre

A high-resolution map of the second 444.4 nm CL peak heights reveals a different heterogeneous pattern across the pearl transect compared to the 551 nm peak, with wider bands of higher and lower intensities and rough textures throughout (Fig. 3A). This indicates that the 444 nm CL signal is likely due to another CL emitter. This peak most closely aligns with a peak from previous studies attributed to “structural defects” (Fig. 1C; Toffolo et al. 2019). In a cave flowstone aragonite sample, broad 440 nm and 520 nm peaks are suggested to be inherent CL of pure aragonite, with the 520 nm peak being 1.5 \times the height of the 440 nm peak (Götte and Richter, 2009). In this study, the average pearl nacre CL signal shows a 551 nm:444 nm peak

ratio of $2.1\times$, since the 551 nm peak has a Mn-driven CL signal contribution, which Götte and Richter suggest occurs at 575 nm (2009; Fig. 1B).

As the 444 nm CL signal is most likely related to the crystal structure itself, rather than a trace element or associated organics, we turn to Raman spectroscopy as a way to probe the carbonate bonding environment in the nacre aragonite. Beyond using Raman spectroscopy as a fingerprinting method to identify different mineral phases in pearls and mollusk shells (Wehrmeister et al. 2007; Soldati et al. 2008; Nehrke et al. 2012), here we interrogate specific Raman modes (see Bischoff et al. 1985; Urmos et al. 1991; Farfan et al. 2021) to determine shifts in the carbonate bonding environment of aragonite across the pearl transects. We observe that the 444 nm CL signal strongly correlates to Raman measurements of the translation (T) and libration (L) modes as expressed as a T:L peak height ratio (Fig. 3B,E; $R^2= 0.34$; $R= 0.58$). This measurement of the T:L peak ratio has been shown to be a function of nacre tablet orientation (Nehrke & Nouet 2011; Wall and Nehrke, 2012; Murphy et al. 2021) and the standard deviation of this ratio may even be used as a measure of relative tablet misorientation (Farfan et al. 2021). Since nacre tablets are laid down radially around the pearl nucleus and extend along the *c*-axis of the aragonite unit cell, shifts in crystallographic orientation observed in the T:L ratio map (Fig. 3B) are perpendicular to the *c*-axis and represent relative shifting views of the *a*- and *b*-axes of the aragonite unit cell. Relative tablet orientation has been shown to reflect environmental temperature (Olson and Gilbert, 2012), but beyond this tablet morphology observation, crystallite orientation cannot give us information about structure defects within the aragonite itself. Thus, we turn to changes in Raman peak widths, which are known to be wider as a function of more disorder within the crystal structure (DeCarlo et al. 2017).

The map of the FWHM values for the dominant v_1 Raman mode visually follows similar patterns observed in the 444 nm CL and Raman T:L ratio maps (Fig. 3C; Supporting Information, Fig. S1), however, v_1 mode FWHMs do not directly correlate with either of these variables via Pearson correlation analyses (Supporting Information, Fig. S8, Table S3). Instead, the v_1 Raman peak FWHM moderately positively correlates with nacre sulfur concentrations for both this study and for Farfan et al. 2021 (Fig. 3F; $R= 0.4$). Sulfate as SO_3^{2-} is well-known to incorporate into the aragonite structure as a substitute for the carbonate groups (CO_3^{2-}) as “carbonate-associated sulfate” (CAS; Pingitore et al. 1994; Farfan et al. 2018; Barkan et al. 2020), which could be a mechanism for crystallographic disorder in nacre, even in freshwater systems. The 444 nm CL signal itself is moderately positively correlated with Kentucky Lake sulfate concentrations and redox potential, which further supports the potential influence of sulfur in nacre mineralogy (Fig. 3 G,H).

Unlike the positive correlations between the 444 nm CL signal and potential sulfur-driven mechanisms for disorder, we observe that wider FWHM of the T mode Raman peaks moderately negatively correlate with the 444 nm CL signal for both this study and for Farfan et al. 2021 (Fig. 3D,I; $R= -0.41$, $R= -0.57$, respectively). The reason the two studies are offset with respect to FWHM values is because they were collected using different collection parameters (i.e. objectives, gratings) which has been shown to have an impact on this value (DeCarlo et al. 2017). Despite being a freshwater system, sodium incorporation in this pearl nacre also displays similar map patterns to Mn and S (Supporting Information, Fig. S2). Na EPMA wt% values are positively correlated with the dominant v_1 Raman mode peak height for this study and for Farfan

et al. 2021 ($R = 0.35\text{--}0.36$; Supporting Information, Fig. S9). Since peak height indicates the intensity of the signal, higher concentrations of Na aligned with higher ν_1 Raman mode heights suggests that Na concentration is proportional to the relative amount of aragonite in each region of the pearl.

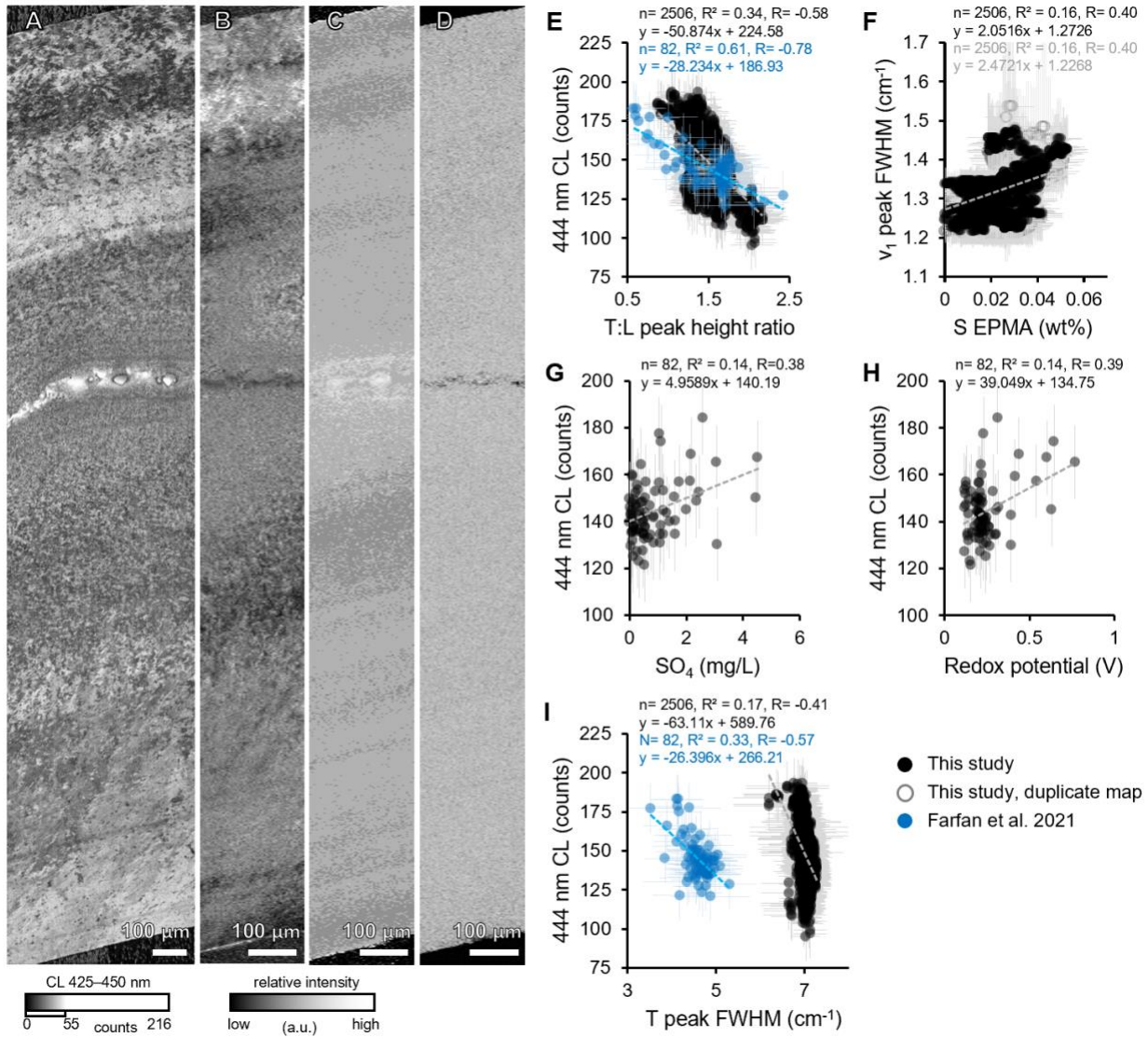


Figure 3. Ultra-high resolution maps along pearl transects of A) CL counts for the 425–450 nm wavelengths that represents the dominant 444 nm CL peak collected at 1×1 μm pixel resolution. Raman spectroscopy maps (3×6 μm pixels) of B) T:L peak height ratios, C) ν_1 mode peak full width at half maximum (FWHM) values, and D) T mode peak (140–170 cm⁻¹) FWHM. E) the 444 nm CL signal as a function of the T:L peak height ratio for this study (black) and a previous study (Farfan et al. 2021, blue). F) The ν_1 mode peak height as a function of sulfur concentration measured by EPMA. Relationships between the 444 nm CL signal as a function G) Kentucky Lake sulfate concentration, H) Kentucky Lake redox potential, and I) Raman T mode peak

FWHM. Values for Kentucky Lake environmental variables are from Farfan et al. 2021 and originally sourced from the Kentucky Lake Long-Term Monitoring Program. All values can be accessed in Supporting Information Table S1 and statistical significance (p-values), Pearson correlation coefficients (R), and linear regressions (R^2) between all variables in this study are in Supporting Information Table S3.

Conclusions

We show that ultrahigh-resolution cathodoluminescence and Raman mapping are powerful tools to observe sub-seasonal shifts in nacre mineralogy, geochemistry, and organic contents. Our results build on previous studies that suggest that the dominant 551 nm CL signal is most likely due to Mn^{2+} that is bound both in organics as well as substituted within the aragonite structure. By combining CL with Raman spectroscopy, we are able to show that the 551 CL signal is closely correlated with the Raman background fluorescence typically associated with organics. In contrast, the secondary 444 nm CL peak signal displays a distinct heterogeneous pattern across the pearl transect that does not match the 551 nm signal and instead is correlated with the Raman-based T:L ratio (a measure of tablet orientation) as well as environmental data from Kentucky Lake for sulfate and redox potential. It is possible that carbonate-associated sulfate may play a role in the crystallographic distortions in aragonite that lead to this 444 nm CL signal, but this should be explored more carefully in future studies. Finally, we also observe that Na is moderately correlated with several Raman-based parameters, especially the v_1 mode peak height for aragonite, indicating that it is associated with the aragonite itself. Overall, there are no clear correlations between $\delta^{18}\text{O}_{\text{Arg}}$ measurements and ultrahigh-resolution CL signals or Raman data that would indicate that organics and aragonite crystallography play an influencing role in shifting $\delta^{18}\text{O}_{\text{Arg}}$, suggesting that nacre faithfully records environmental values.

Acknowledgements

WiscSIMS is supported by NSF (EAR-2004618) and the University of Wisconsin-Madison.

References

Barbin, V. (2000). Cathodoluminescence of carbonate shells: biochemical vs diagenetic process. In *Cathodoluminescence in geosciences* (pp. 303-329). Springer, Berlin, Heidelberg.
https://link.springer.com/chapter/10.1007/978-3-662-04086-7_12 Book chapter

Barbin, V. (2013). Application of cathodoluminescence microscopy to recent and past biological materials: a decade of progress. *Mineralogy and Petrology*, 107(3), 353-362.

Barkan, Y., Paris, G., Webb, S. M., Adkins, J. F., & Halevy, I. (2020). Sulfur isotope fractionation between aqueous and carbonate-associated sulfate in abiotic calcite and aragonite. *Geochimica et Cosmochimica Acta*, 280, 317-339.

Barthelat, Z. Yin, M. J. Buehler, Structure and mechanics of interfaces in biological materials. *Nat. Rev. Mater.* 1, 1–16 (2016).

Banerjee, A., & Habermann, D. (2000). Identification of Chinese fresh-water pearls using MN 2+ activated cathodoluminescence. *Carbonates and Evaporites*, 15(2), 138-148.
<https://www.proquest.com/openview/22e7206fa7f3eb9dfd4c9eb10995c0bc/1?pq-origsite=gscholar&cbl=2043947>

Bischoff, W. D., Sharma, S. K., & MacKenzie, F. T. (1985). Carbonate ion disorder in synthetic and biogenic magnesian calcites: A Raman spectral study. *American Mineralogist*, 70(5–6), 581–589.

Bourrat X, Li Q, Feng Q, Angellier M, Dissaux A, Beny J, Barbin V, Stempflé P, Rousseau M, Lopez E (2012) Origin of growth defects in pearl. *Mater Charact* 72:94–103
<https://core.ac.uk/download/pdf/54037779.pdf>

Carré, M., Bentaleb, I., Bruguier, O., Ordinola, E., Barrett, N. T., & Fontugne, M. (2006). Calcification rate influence on trace element concentrations in aragonitic bivalve shells: evidences and mechanisms. *Geochimica et Cosmochimica Acta*, 70(19), 4906-4920.

DeCarlo, T. M., D'Olivo, J. P., Foster, T., Holcomb, M., Becker, T., & McCulloch, M. T. (2017). Coral calcifying fluid aragonite saturation states derived from Raman spectroscopy. *Biogeosciences*, 14(22), 5253–5269. <https://doi.org/10.5194/bg-14-5253-2017>

DeCarlo, T. M., Ren, H., & Farfan, G. A. (2018). The origin and role of organic matrix in coral calcification: insights from comparing coral skeleton and abiogenic aragonite. *Frontiers in Marine Science*, 5, 170.

Eaton-Magaña, S., Breeding, C. M., Palke, A. C., Homkraje, A., Sun, Z., & McElhenny, G. (2021). Raman and photoluminescence mapping of gem materials. *Minerals*, 11(2), 177.

England, J., Cusack, M., Paterson, N. W., Edwards, P., Lee, M. R., & Martin, R. (2006). Hyperspectral cathodoluminescence imaging of modern and fossil carbonate shells. *Journal of Geophysical Research: Biogeosciences*, 111(G3).
<https://agupubs.onlinelibrary.wiley.com/doi/epdf/10.1029/2005JG000144>

Espinosa et al., Tablet-level origin of toughening in abalone shells and translation to synthetic composite materials. *Nat. Commun.* 2, 173 (2011).

Farfan, G. A., Apprill, A., Webb, S. M., & Hansel, C. M. (2018). Coupled X-ray fluorescence and X-ray absorption spectroscopy for microscale imaging and identification of sulfur species within tissues and skeletons of scleractinian corals. *Analytical chemistry*, 90(21), 12559-12566.

Farfan, G. A., Zhou, C., Valley, J. W., & Orland, I. J. (2021). Coupling mineralogy and oxygen isotopes to seasonal environmental shifts recorded in modern freshwater pearl nacre from Kentucky Lake. *Geochemistry, Geophysics, Geosystems*, 22(12), e2021GC009995.

Gaft, M., Reisfeld, R., & Panczer, G. (2015). *Modern luminescence spectroscopy of minerals and materials*. Springer.

Hänsch, R., & Mendel, R. R. (2009). Physiological functions of mineral micronutrients (cu, Zn, Mn, Fe, Ni, Mo, B, cl). *Current opinion in plant biology*, 12(3), 259-266.

Jeffree, R. A., Markich, S. J., Lefebvre, F., Thellier, M., & Ripoll, C. (1995). Shell microlaminations of the freshwater bivalve *Hyridella depressa* as an archival monitor of manganese water concentration: experimental investigation by depth profiling using secondary ion mass spectrometry (SIMS). *Experientia*, 51(8), 838-848.

Micro-laminations of Mn a function of lake Mn concentrations

Linzmeier, B. J., Kozdon, R., Peters, S. E., Valley, J. W. (2016). Oxygen isotope variability within growth bands suggests daily depth migration behavior is recorded in *Nautilus* shell aragonite, *PLoS One*, 1-31. <https://doi.org/10.1371/journal.pone.0153890>

Murphy, A. E., Jakubek, R. S., Steele, A., Fries, M. D., & Glamoclija, M. (2021). Raman spectroscopy provides insight into carbonate rock fabric based on calcite and dolomite crystal orientation. *Journal of Raman Spectroscopy*, 52(6), 1155-1166.

Nehrke, G., & Nouet, J. (2011). Confocal Raman microscope mapping as a tool to describe different mineral and organic phases at high spatial resolution within marine biogenic carbonates: case study on *Nerita undata* (Gastropoda, Neritopsina). *Biogeosciences*, 8(12), 3761-3769.

Nehrke, G., Poigner, H., Wilhelms-Dick, D., Brey, T., & Abele, D. (2012). Coexistence of three calcium carbonate polymorphs in the shell of the Antarctic clam *Laternula elliptica*. *Geochemistry, Geophysics, Geosystems*, 13(5).

Olson, I. C., & Gilbert, P. U. P. A. (2012). Aragonite crystal orientation in mollusk shell nacre may depend on temperature. The angle spread of crystalline aragonite tablets records the water temperature at which nacre was deposited by *Pinctada margaritifera*. *Faraday Discussions*, 159(1), 421-432.

Orland, I. J., Kozdon, R., Linzmeier, B., Wycech, J., Sliwinski, M., Kitajima, K., et al. (2015). Enhancing the accuracy of carbonate $\delta^{18}\text{O}$ and $\delta^{13}\text{C}$ measurements by SIMS. In AGU Fall Meeting Abstracts (Vol. 2015, p. PP52B-03).

Peacock, E., Mitchell, J., & Kirkland, B. (2020). Investigating freshwater mussel (Unionidae) shell diagenesis at an archaeological site on the Tombigbee River, Mississippi, southeastern USA. *Journal of Archaeological Science: Reports*, 31, 102350. https://www.sciencedirect.com/science/article/pii/S2352409X20301413?casa_token=iOWmMDGQZLEAAAAA:SgyAgUA51jXuovaGt2_InqfqZBOzvw5tBPC-HQK2S26SrнDEcYauMF1yi5y4RBNBGt3G8ZjJxXRj

Pingitore Jr, N. E., Meitzner, G., & Love, K. M. (1995). Identification of sulfate in natural carbonates by X-ray absorption spectroscopy. *Geochimica et Cosmochimica Acta*, 59(12), 2477-2483.

Siegele, R., Orlic, I., Cohen, D. D., Markich, S. J., & Jeffree, R. A. (2001). Manganese profiles in freshwater mussel shells. *Nuclear Instruments and Methods in Physics Research Section B: Beam Interactions with Materials and Atoms*, 181(1-4), 593-597.

Soldati, A. L., Jacob, D. E., Wehrmeister, U., Häger, T., & Hofmeister, W. (2008). Micro-Raman spectroscopy of pigments contained in different calcium carbonate polymorphs from freshwater cultured pearls. *Journal of Raman Spectroscopy: An International Journal for Original Work in all Aspects of Raman Spectroscopy, Including Higher Order Processes, and also Brillouin and Rayleigh Scattering*, 39(4), 525-536

Soldati, A. L., Jacob, D. E., Schöne, B. R., Bianchi, M. M., & Hajduk, A. (2009). Seasonal periodicity of growth and composition in valves of *Diplodon chilensis patagonicus* (d'Orbigny, 1835). *Journal of Molluscan Studies*, 75(1), 75-85.

Soldati, A. L., Goettlicher, J., Jacob, D. E., & Vilas, V. V. (2010). Manganese speciation in *Diplodon chilensis patagonicus* shells: a XANES study. *Journal of Synchrotron Radiation*, 17(2), 193-201.

Soldati, A. L., Jacob, D. E., Glatzel, P., Swarbrick, J. C., & Geck, J. (2016). Element substitution by living organisms: the case of manganese in mollusc shell aragonite. *Scientific Reports*, 6(1), 1-9.

Sommer, S. E. (1972). Cathodoluminescence of carbonates, 1. Characterization of cathodoluminescence from carbonate solid solutions. *Chemical Geology*, 9(1-4), 257-273.
<https://www.sciencedirect.com/science/article/abs/pii/0009254172900642>

Southgate, P., & Lucas, J. (Eds.). (2011). *The pearl oyster*. Elsevier.

Takesue, R. K., Bacon, C. R., & Thompson, J. K. (2008). Influences of organic matter and calcification rate on trace elements in aragonitic estuarine bivalve shells. *Geochimica et Cosmochimica Acta*, 72(22), 5431-5445.

Toffolo, M. B., Ricci, G., Caneve, L., & Kaplan-Ashiri, I. (2019). Luminescence reveals variations in local structural order of calcium carbonate polymorphs formed by different mechanisms. *Scientific reports*, 9(1), 1-15.
<https://www.nature.com/articles/s41598-019-52587-7>

Toffolo, M. B. (2021). The significance of aragonite in the interpretation of the microscopic archaeological record. *Geoarchaeology*, 36(1), 149-169.
<https://onlinelibrary.wiley.com/doi/epdf/10.1002/gea.21816>

Urmos, J., Sharma, S. K., & Mackenzie, F. T. (1991). Characterization of some biogenic carbonates with Raman spectroscopy. *American Mineralogist*, 76(3-4), 641-646.

van der Schatte Olivier, A., Jones, L., Vay, L. L., Christie, M., Wilson, J., & Malham, S. K. (2020). A global review of the ecosystem services provided by bivalve aquaculture. *Reviews in Aquaculture*, 12(1), 3-25.

Vihtakari, M., Renaud, P. E., Clarke, L. J., Whitehouse, M. J., Hop, H., Carroll, M. L., & Ambrose, W. G., Jr. (2016). Decoding the oxygen isotope signal for seasonal growth patterns in Arctic bivalves. *Palaeogeography, Palaeoclimatology, Palaeoecology*, 446, 263–283.

Wall, M., & Nehrke, G. (2012). Reconstructing skeletal fiber arrangement and growth mode in the coral *Porites lutea* (Cnidaria, Scleractinia): a confocal Raman microscopy study. *Biogeosciences*, 9(11), 4885–4895.

Wehrmeister, U., Jacob, D. E., Soldati, A. L., Hager, T., & Hofmeister, W. (2007). Vaterite in freshwater cultured pearls from China and Japan. *JOURNAL OF GEMMOLOGY-LONDON-*, 30(7/8), 399.

*Wycech, J., Kelly, D. C., Kozdon, R., Orland, I., Spero, H. J., & Valley, J. W. (2018). Comparison of $\delta^{18}\text{O}$ analyses on individual planktic foraminifer (*Orbulina universa*) shells by SIMS and gas-source mass spectrometry. Chemical Geology*, 483, 119–130. <https://doi.org/10.1016/j.chemgeo.2018.02.028>